Received: 25 June 2018 | Revised: 21 February 2019 | Accepted: 6 March 2019

DOI: 10.1002/jcp.28503

ORIGINAL RESEARCH ARTICLE

WILEY Journal of Cellular Physiology

Functional suppression of Epiregulin impairs angiogenesis and aggravates left ventricular remodeling by disrupting the extracellular-signal-regulated kinase1/2 signaling pathway in rats after acute myocardial infarction

Ying Cai[1] | Kang-Ling Xie[2] | Huan-Lin Wu[2] | Kai Wu[1]

[1]Department of Rehabilitation, Xiangya Hospital, Central South University, Changsha, P.R. China

[2]Second School of Clinical Medicine, Guangzhou University of Chinese Medicine, Guangzhou, P.R. China

Correspondence
Kai Wu, Department of Rehabilitation, Xiangya Hospital, Central South University, No. 87, Xiangya Road, 410008 Changsha, Hunan, P.R. China.
Email: wkwoolongqq@163.com

Abstract

Acute myocardial infarction (AMI), a severe consequence of coronary atherosclerotic heart disease, is often associated with high mortality and morbidity. Emerging evidence have shown that the inhibition of the extracellular-signal-regulated kinase (ERK) signaling pathway appears to protect against AMI. Epiregulin (EREG) is an autocrine growth factor that is believed to activate the MEK/ERK signaling pathway. Therefore, the aim of the present study was to determine the expression patterns of EREG in AMI and to further study its effects on AMI induced experimentally in rats focusing on angiogenesis and left ventricular remodeling. Microarray-based gene expression profiling of AMI was used to identify differentially expressed genes. To understand the biological significance of EREG and whether it is involved in AMI disease through the ERK1/2 signaling pathway, rats after AMI were treated with small interfering RNA (siRNA) against EREG, an ERK1/2 pathway inhibitor, PD98059, or both of them. The microarray data sets GSE66360 and GSE46395 showed that EREG was robustly induced in AMI. Both siRNA-mediated depletion of EREG and PD98059 treatment were shown to significantly increase infarct size and left ventricular cardiomyocyte loss and enhance left ventricular remodeling. In addition, we also found that the ERK1/2 signaling pathway was inhibited following siRNA-mediated EREG inhibition and PD98059 could enhance the effects of EREG inhibition on AMI. In conclusion, these findings highlight that the silencing of EREG inhibits angiogenesis and promotes left ventricular remodeling by disrupting the ERK1/2 signaling pathway, providing a novel therapeutic target for limiting AMI.

KEYWORDS

acute myocardial infarction, angiogenesis, EREG, ERK1/2, ventricular remodeling

1 | INTRODUCTION

Atherosclerotic-induced coronary occlusion is the primary cause of acute myocardial infarction (AMI), therefore the main treatment strategy is instant restoration of a patent coronary artery by mechanically or thrombolytic and antiplatelet therapies, as well as injection of agents that diminish oxygen consumption and stimulate the heart muscle (Zouggari et al., 2013). The pathogenesis and course of AMI are strongly associated with various risk factors, and the associated factors of morbidity and mortality are widely considered to be increased by smoking (Sivaraman, Zachariah, & Annamala, 2014). During its acute stage, the ischemic and infarcted myocardium of patients induces a remarkable enhancement of the inflammatory response and oxidative stress (Yuan et al., 2013). Furthermore, patients with severe AMI still

have a high risk of heart failure progression during ventricular remodeling after initial ischemia and reperfusion treatments (Seropian, Toldo, Van Tassell, & Abbate, 2014). Currently, reperfusion therapy can be regarded as the standard methods for treating AMI, but it may lead to reperfusion injury such as worsening tissue damage or paradoxical cardiomyocyte dysfunction (Neri, Riezzo, Pascale, Pomara, & Turillazzi, 2017). Prognosis improvement and timely interventions of AMI require that the differential diagnoses are finalized in an accurate and rapid fashion, but this is a complex task to achieve with many factors requiring adequate consideration (Jia et al., 2016). Therefore, it is necessary to explore the effect of gene silencing on the treatment of AMI.

Epiregulin (EREG) belongs to the epidermal growth factor (EGF) family that comprises betacellulin and neuregulins, transforming growth factor-α, heparin-binding EGF-like growth factor, amphiregulin (AREG), and epigen (Yun et al., 2012). EREG is one of the ligands of the EGF receptor (EGFR), with reports indicating that their interactions exert influence on the activation of the dorsal root ganglion neurons generating pain behaviors (Martin et al., 2017). EREG, as one of the molecules implicated in literature in the process of glioma malignancy, contributes to enhanced tumorigenicity via the activation of the extracellular-signal-regulated kinase (ERK) pathway and mitogen-activated protein kinase (MAPK) pathway in glioblastoma (Kohsaka et al., 2014). The ERK pathway exerts a significant effect on the meditation of waking neuromodulators on gene expression based on the pharmacological restraint of a large array of signaling pathways controlling gene expression (Mikhail, Vaucher, Jimenez, & Tafti, 2017). Moreover, the ERK1/2 signaling pathway has been previously reported to be associated with various cellular functions (transformation, differentiation, and proliferation) together with the MAPK signaling pathway (Lake, Correa, & Muller, 2016). However, the role of the EREG-mediated ERK1/2 signaling pathway in rats with AMI remains largely unknown. Therefore, the aim of the current study was to clarify whether small interfering RNA (siRNA)-mediated downregulation of EREG and ERK inhibition confer promotive effects over myocardial injury in rats with AMI, with emphasis placed on angiogenesis and ventricular remodeling.

2 | METHODS AND MATERIALS

2.1 | Ethics statement

The current study was performed in strict accordance with the *Guide for Care and Use of Laboratory Animals* of the National Institutes of Health. The protocol was approved by the Institutional Animal Care and Use Committee of Xiangya Hospital, Central South University, with extensive efforts made to minimize animal suffering as well as the number of animals used in the study.

2.2 | Microarray-based gene expression profiling

Myocardial infarction (MI)-related microarray expression data (GSE66360 and GSE46395) and gene probe annotation files were obtained from Gene Expression Omnibus (GEO; https://www.ncbi.nlm.nih.gov/geo/) to screen out differentially expressed genes (DEGs). The GSE66360 data set included the differential expression of circulating endothelial cells from 50 healthy individuals as well as 49 patients with AMI, with the annotation platform GPL-[HG-U133_Plus_2] Affymetrix Human Genome U133 Plus 2.0 Array. The GSE46395 data set covered the differential expression of normal mice, whereas the AMI mouse models were established by ligating the anterior interventricular artery, in connection with the GPL10787-Agilent-028005 SurePrint G3 Mouse GE 8×60K Microarray (Probe Name version) annotation platform. The microarray expression data were preprocessed to screen the DEGs, followed by construction of a heat map using the limma package of R software (Smyth, 2004). $p < 0.05$ and (log [fold change]) > 2 were set as the threshold. Venn analysis was performed using calculate and draw custom Venn diagrams (http://bioinformatics.psb.ugent.be/webtools/Venn/), which was used to compare the DEGs of the two aforementioned data sets. A comprehensive database of information on human-disease-related genes and mutations DisGeNET (http://www.disgenet.org/web/DisGeNET/menu/search?4) was used to search MI-related genes. The mutual interaction of DEGs and MI-related genes was obtained using the String database (https://string-db.org/), and gene interaction network was plotted using the Cytoscape 3.6.0 software (Shannon et al., 2003).

2.3 | Animal treatment

Sixty specific pathogen-free (SPF) Wistar rats weighing between 200 and 275 g were included in this experimental study. The animals were housed in temperature- (22–25°C) and humidity-controlled rooms after a 1-week period of acclimatization before the study. Next, 50 rats were used to establish AMI models, and the remaining 10 rats received no treatment (the normal group). The model establishment process had a 40% mortality rate, with 30 rats successfully modeled and divided into 5 groups (6 rats in each group) for adenovirus injection and the following experiment: the model group (without injection), the negative control group (injected with adenovirus of negative nonsense sequence), the EREG-siRNA group (injected with adenovirus of siRNA against EREG), the PD98059+EREG-siRNA group (injected with PD98059, an ERK1/2 signaling pathway inhibitor and adenovirus of siRNA against EREG), and the PD98059 group (injected with PD98059). Adenovirus was intramyocardially injected into the site around the infarcted region of the heart (Wang et al., 2012).

2.4 | AMI model establishment

SPF male rats were intraperitoneally injected with 3% pentobarbital sodium at 60 mg/kg, with the hair overlying the chest and neck region shaved 4 min later. Next, the disinfected skin was dissected (length 1–2 cm) to expose the cardiac organs, followed by the insertion of a trachea cannula connected to a breathing machine (frequency of 20–30 times/min, respiratory quotient of 1:1, tidal volume of 7 ml/kg). The chest and neck skin regions were disinfected after the

muscles had been bluntly separated, after which the third and fourth ribs were dissected allowing the chest to expand and further expose the cardiac organs. Next, the pericardium was dissected, with a ligation made between the arterial cone and left auricle with 0 line. Finally, ischemic echocardiogram (ECG) changes were regarded to be reflective of successful ligation of the left anterior descending coronary artery, resulting in successful AMI model establishment (Fernandez Machulsky et al., 2017). In addition, a raised ST-segment >0.2 mV for 30 min upon ECG examination was considered to be indicative of successful AMI model establishment. After operation, six heart samples were collected from each group to evaluate cardiac function indicators leading to rat death and sample screening.

2.5 | Evaluation of cardiac function indicators

Japanese Aloka color doppler ultrasound diagnostic apparatus (Aloka5500; L5410 linear probe, transducer frequency of 13 MHz) was used. After the rats had been anesthetized with 3% pentobarbital sodium (100 g/0.1 ml; Beijing Propbs Biotechnology Co., Ltd., Beijing, China), ECGs were obtained 4-weeks postsurgical procedure. Rat morphological indicators included left ventricular end-diastolic diameter (LVEDD) and left ventricular end-systolic diameter (LVESD) as well as systolic function indicators, with left ventricular ejection fraction (LVEF) and left ventricular fractional shortening (LVFS) also recorded.

2.6 | Hematoxylin–eosin staining

Initially, 7 days after MI operation, the partial heart tissues of the infarcted and noninfarcted rats were fixed with 10% formaldehyde, dehydrated with gradient ethanol (70%, 80%, 90%, 95%, and 100% respectively; 2 hr/time), cleared two times with dimethylbenzene (5 min/time), immersed, embedded with paraffin, and finally sliced into 4-μm sections. The ischemic myocardium tissues on the margin of the infarcted area in the AMI rats and left ventricular myocardial tissues from the normal rats were collected, dewaxed, and hydrated, stained with hematoxylin, differentiated with 1% hydrochloric-alcohol solution. After being counterstained with eosin, the tissues were dehydrated using gradient ethanol, cleared by dimethylbenzene, and mounted with gum. A total of five high-power fields were randomly selected to analyze the morphological characteristics of AMI infarcted tissues.

2.7 | Determination of hemodynamic parameters

Seven days after operation, the rats were anesthetized intraperitoneally and fixed in a supine position. An incision was subsequently made to the neck, which was followed by blunt dissection of the subcutaneous tissues to expose the carotid artery. Next, after the far-end of the carotid artery had been ligated, the near-end was clamped using a vascular clamp, with the right carotid artery punctured using a 20-G indwelling artery needle. After successful puncturing, the needle was removed, and the vascular clamp was loosened, followed by the insertion of a sheathing canal into the carotid artery providing access to the aorta. Heparin was then injected for anticoagulation purposes, followed by the use of the BL-420E biofunctional experiment system. The hemodynamics module was then used after the sheathing canal had been connected with the pressotransducer. Finally, after stable conditions had been confirmed, left ventricular systolic pressure (LVSP), left ventricular end-diastolic pressure (LVEDP), and left ventricular maximum increase and decrease rates (±dp/dtmax) were measured and recorded.

2.8 | Immunofluorescence staining

The myocardial tissues of the ischemic myocardium at the edge of infarct area and the left ventricular tissues of normal rats were paraffin-embedded, sectioned, dewaxed conventionally, and underwent antigen retrieval under high-temperature and high-pressure conditions using a citric buffer after washing. Next, the slices were immersed in 3% H_2O_2 at room temperature for 15 min for peroxidase inactivation purposes. After three rinses with phosphate-buffered saline (PBS; 2 min/time), the slices were blocked with serum (1:10) and then incubated in a humidified box for 20 min at 37°C. The excess liquids were removed without washing. Afterward, the tissue slices were incubated with the monoclonal mouse anti-rat antibody to cell adhesion molecule (CD31; 1: 200; ab119339; Abcam Inc., Cambridge, MA) and polyclonal rabbit anti-rat antibody to α-smooth muscle actin (α-SMA; 1: 100; BD-PT5053; Beijing Biodragon Immunotechnologies Co., Ltd., Beijing, China) in a humidified box for 1 hr at 37°C. After three PBS washes (3 min/time), the slices were incubated with goat anti-mice fluorescein-isothiocyanate-labeled immunoglobulin G (IgG; 1: 32; G11372; Beijing Bellancom Chemistry, Beijing, China) and goat anti-rabbit CY3-labeled IgG (1: 50, YB1123; Shanghai Yubo Biological Technology Co., Ltd., Shanghai, China) in a humidified box for 2 hr at 37°C. The slices were then stained with 4′,6-diamidino-2-phenylindole solution (C1005; Beyotime Biotechnology Co., Shanghai, China) under conditions void of light for nuclear staining, rinsed with PBS, and blocked with a fluorescence quenching agent. A total of five fields (200×) were randomly selected for observation using a fluorescence microscope (FV1200; Olymupus Optical Co., Ltd., Tokyo, Japan).

2.9 | 2,3,5-Triphenyl-2H-tetrazolium chloride assay

The collected rat hearts were washed with ice salt water to remove the excess blood from the surface and inside the ventricle with saline, from which the atrium and right ventricle were dissected. The ischemic area was immediately controlled after the ligation of the anterior descending branch of the left coronary artery. The left ventricle (LV) was evenly sliced into five 1-mm cross sections and subsequently incubated with 1% 2,3,5-triphenyl-2H-tetrazolium chloride (TTC) solution (2530-85-0; Guidechem Co., Ltd., Shanghai, China), under conditions void of light for 10 min at 37°C and fixed in 4% formalin solution overnight. Viable myocardium exhibited red color, and the infarcted tissue was stained white. The infarct area and

the total LV area were measured using the Image Analysis Software Image-Pro Plus 6.0. The percentage of MI area = (total of MI area/total of myocardial area) × 100% (Oyama et al., 2004).

2.10 | TdT-mediated dUTP-biotin nick-end labeling staining

The paraffin-embedded slices obtained from heart tissues of the rats were incubated at room temperature for 10 min with 3% H_2O_2, washed three times with distilled water (2 min/time), detached with protease K (20 μg/mL; MB3060; Meilunbio; Dalian, Liaoning, China) for 30 min at 37°C, and rinsed three times with PBS (2 min/time). After reaction with 3% H_2O_2 for 5 min at room temperature to quench endogenous peroxidase activity, the slices were rinsed three times with PBS (2 min/time), and mixed with 0.1% citric acid solution containing 0.1% TritonX-100 (FK-YJ1057; Fan Ke Biotechnology Co., Ltd., Shanghai, China). The slices were then placed on ice for 4 min and rinsed three times with PBS (2 min/time). The slices were then permitted to react with 50 μl of TdT-mediated dUTP-biotin nick-end labeling (TUNEL) solution (ZK-8005; Beijing Zhongshan Jinqiao Biotechnology Co., Ltd., Beijing, China) for 1 hr at 37°C, followed by three PBS washes (2 min/time) and stained with diaminobenzidine/H_2O_2 color-substrate solution (Invitrogen, Shanghai, China) for 5 min at room temperature. The reaction was then terminated by washing, with the slices subsequently counter-stained with hematoxylin, dehydrated, cleared, and mounted. Finally, five nonoverlapping views were randomly selected for observation under an optical microscope to calculate the TUNEL-positive cells of rat heart issues in each group, after which the average value was obtained. The rate of apoptosis was expressed as the percentage of apoptotic cells to the total cells.

2.11 | Reverse transcription-quantitative polymerase chain reaction

The total RNA content was extracted using Trizol reagent (16096020; Thermo Fisher Scientific Inc., Waltham, MA). The obtained RNA (5 μg) was reversely transcribed into complementary DNA (cDNA) in accordance with the instructions of the TaqMan MicroRNA Assays Reverse Transcription Primer (4427975; Applied Biosystems, Inc., Foster City, CA). Next, cDNA was used for reverse transcription, diluted to 50 mg/μl, with 2 μl added each time. The reaction conditions were performed with a total volume of 25 μl as follows: 1.0 μl of DNA, 2.5 μl of 10× polymerase chain reaction (PCR) buffer solution, 2.0 μl of dNTPs, 2.5 μl of forward primer, and 2.5 μl of reverse primer, 0.5 μl of Taq enzyme (S10118; Shanghai Yuanye biotechnology Co., Ltd., Shanghai, China), and 13 μl of ddH_2O. The reaction conditions were conducted according to the following: predenaturation at 94°C for 5 min, 30 cycles of denaturation at 94°C for 30 s, annealing at 54.5°C for 30 s, extension at 72°C for 30 s, and final extension at 72°C for 10 min, followed by preservation at 4°C. The primer sequences of EREG, ERK1/2, vascular endothelial growth factor (VEGF), basic fibroblast growth factor (bFGF) and insulin-like growth factor I (IGF-I) are illustrated in Table 1. Glyceraldehyde-3-phosphate dehydrogenase was regarded as the internal reference. The ratio of the target gene between the experimental and control groups was calculated using the $2^{-\Delta C_t}$ method. The messenger RNA (mRNA) expression of each gene was determined according to the following formula: $\Delta C_t = C_{t\ \text{target gene}} - C_{t\ \text{internal gene}}$ and mRNA relative transcription level = $2^{-\Delta C}t$. C_t was considered to be reflective of the amplified cycle number when the real-time fluorescence intensity of reaction reaches the set threshold. The experiment was conducted three times.

TABLE 1 Primer sequences for reverse transcription-quantitative polymerase chain reaction

Gene	Primer sequence (5′–3′)
EREG	F: AGGGGTTTTAGAAGGAAGGC R: TATCAATAATTCAAACGCCCTC
ERK1	F: CCAGAGTGGCTATCAAGAAG R: TCCATGAGGTCCTGAACAA
ERK2	F: TGCCGTGGAACAGGTTGT R: TGGGCTCATCACTTGGGT
VEGF	F: CCGCAGACGTGTAAATGTTCC R: GACGGTGACGATGGTGGTGT
bFGF	F: GAGCGACCCTCACATCAA R: CGTTTCAGTGCCACATACC
IGF-I	F: GGAGGCTGGAGATGTACTGTGCT R: TGTGTTCTTCAAGTGTACTTCCTTCTG
GAPDH	F: TCAACTACATGGTCTACATGTTCCAG R: TCCCATTCTCAGCCTTGACTG

Note. bFGF: basic fibroblast growth factor; EREG: epiregulin; ERK1: extracellular-regulated protein kinases 1 and 2; F: forward; GAPDH: glyceraldehyde-3-phosphate dehydrogenase; IGF-I: insulin-like growth factor I; R: reverse; VEGF: vascular endothelial growth factor .

2.12 | Western blot analysis

The sliced sections obtained from heart tissues of the rats were treated with cell lysis buffer (100 mg/100 μl; BB-3209; Bestbio Co., Ltd., Shanghai, China), homogenized on ice, followed by lysis for 30 min in a refrigerator at 4°C. The lysate was then centrifuged in a refrigerated microcentrifuge tube for 5 min at 12,000 r/min at 4°C. After collection of the supernatant, a bicinchoninic acid kit (20201ES76; Yeasen Biotechnology Co., Ltd., Shanghai, China) was used to determine the protein concentration in the tissues. A total of 50 μg of protein was dissolved in the buffer solution and boiled at 100°C for 5 min. After 10% sodium dodecyl sulfate polyacrylamide gel electrophoresis, protein samples were transferred onto a nitrocellulose membrane via the wet transfer method and blocked with Odyssey blocking solution at 4°C overnight. The primary antibodies, rabbit polyclonal antibody to EREG (RN206184; Beijing OriGene Technologies Co., Ltd., Beijing, China), rabbit polyclonal antibody to ERK1/ERK2 (1:1,000; ab17942), rabbit polyclonal antibody to VEGF (1:1,000; ab46154; Abcam Inc., Shanghai, China), mouse monoclonal antibody to bFGF (1:500; sc-136255; Santa Cruz Biotechnology, Dallas, TX), and mouse monoclonal antibody to IGF-I (1:5,000; ab36532; Abcam Inc., Shanghai, China) were added to the membrane for overnight incubation, which were then rinsed three

times with PBS at room temperature (5 min/time). Next, after the addition of the secondary antibody, horseradish-peroxidase-conjugated goat anti-rabbit (PB001; 1:200; Shanghai Immune Biotech Co., Ltd., Shanghai, China), the membrane was incubated for 1 hr at 37°C, followed by three PBS washes at room temperature (5 min/time). After reaction with an enhanced chemiluminescence solution (ECL808-25; Biomiga, San Diego, CA) for 1 min at room temperature, the solution was discarded, and the membrane was covered with a plastic wrap and exposed to X-ray (36209ES01; Qian Chen Biotechnology Co., Ltd., Shanghai, China). A gel document system was used to analyze the optical density (OD) of the protein bands. The relative contents of the target protein = average OD of target protein/average OD of the internal reference. The experiment was repeated three times.

2.13 | Statistical analysis

Statistical analyses were performed using the SPSS 21.0 statistical software (IBM Corp., Armonk, NY). Measurement data were expressed as mean ± standard deviation, with the normal distribution among multiple groups evaluated using the Kolmogorov–Smirnov test. Comparisons of data obeying normal distribution between multiple groups were assessed by one-way analysis of variance, and the least significant difference test was applied for pairwise comparisons. Comparisons of data with skewed distribution were analyzed using nonparametric the Kruskal–Wallis test. $p < 0.05$ was considered to be statistically significant.

3 | RESULTS

3.1 | EREG may participate in the progression of AMI through the regulation of the ERK1/2 signaling pathway

MI-related gene expression chips GSE66360 and GSE46395 from the GEO database were utilized to screen out DEGs with $p < 0.05$ and (log [fold change] > 2 as the threshold. A Venn map was plotted by comparing the top 70 DEGs between the two chips (Figure 1a). The

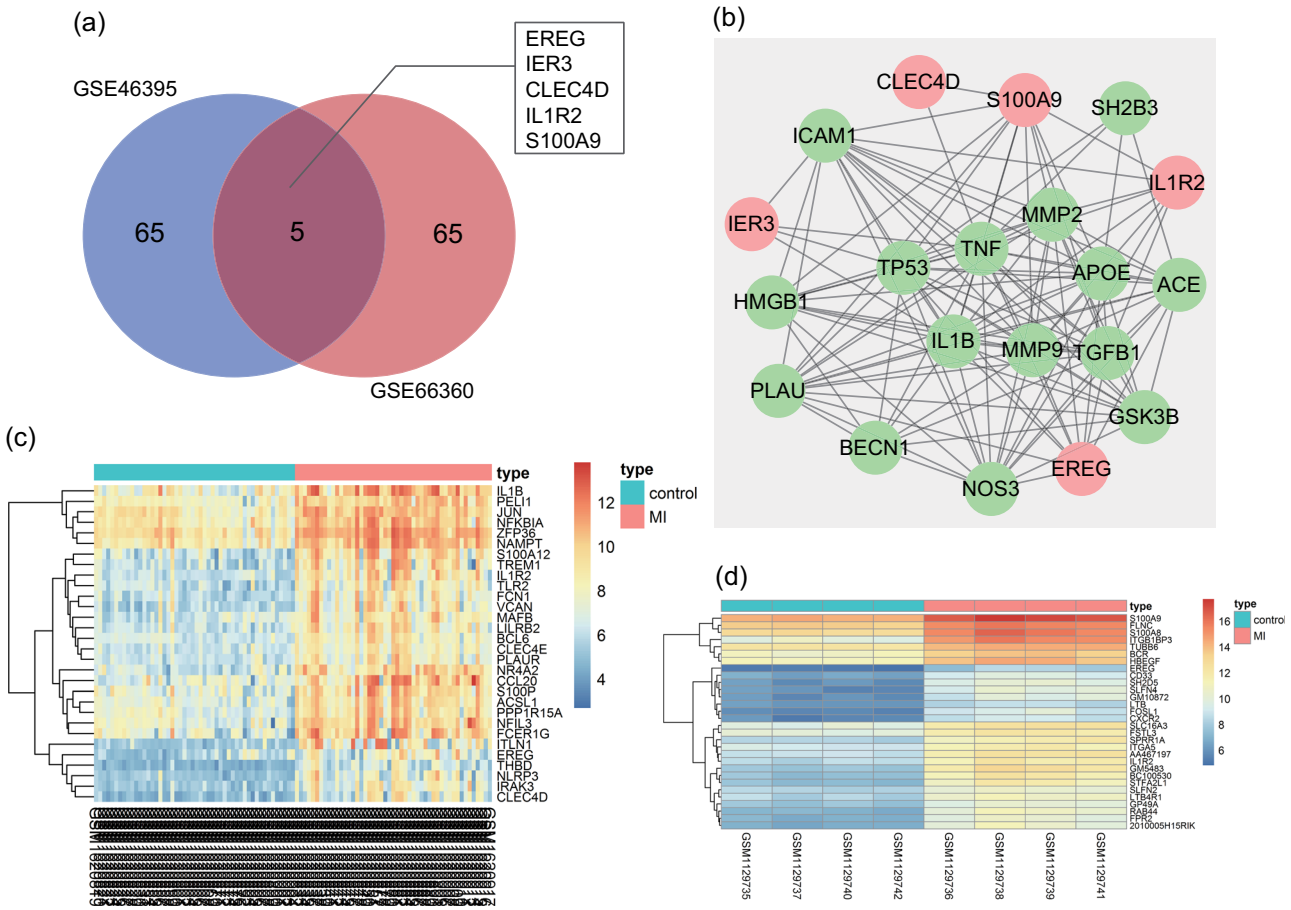

FIGURE 1 EREG is involved in MI disease in an ERK1/2-signaling-pathway-dependent manner. (a) Analysis of the top 70 DEGs between GSE66360 and GSE46395 data sets; (b) Interaction between MI-related DEGs and disease genes, where green circle represents MI disease genes, and red circle represents MI-related DEGs. (c) and (d) The expression heat maps of top 30 DEGs in GSE66360 and GSE46395, with sample number as the abscissa and DEGs as the ordinate; upper right histogram is color gradation where every rectangle corresponds to a sample expression value; red shows high expression whereas green represents the low expression. EREG: epiregulin; DEGs: differentially expressed genes; ERK1, extracellular-regulated protein kinases 1/2; MI: myocardial infarction [Color figure can be viewed at wileyonlinelibrary.com]

data demonstrated five intersecting genes (EREG, IER3, CLEC4D, IL1R2, and S100A9), which were used for the following analysis. The top 15 MI-related genes, obtained from the DisGeNET database with "Myocardial Infarction" as the keyword, were considered to be disease genes. On the basis of protein–protein interaction information obtained from the String database, the identified relationship between disease genes and DEGs was analyzed, with the interaction network subsequently plotted (Figure 1b). The results indicated that S100A9 and EREG had a direct impact on various disease genes, suggesting its correlation with MI. Furthermore, S100A9 was demonstrated to be highly expressed in MI (Du et al., 2012). Through expression heat maps of the top 30 DEGs in the chip GSE66360 (Figure 1c) as well as that of the top 30 DEGs in the chip GSE46395 (Figure 1d), an abnormally high expression of EREG was detected in MI. Previous studies have repeatedly highlighted the notable role of the ERK1/2 signaling pathway in MI (Wei et al., 2015, Yu, Wei, Zhang, Weiss, & Felder, 2016), with EREG reported to activate the ERK1/2 signaling pathway (Fang, Cheng, Chang, Sun, & Leung, 2013). Therefore, the current study highlighted the significant role of EREG in MI through the ERK1/2 signaling pathway.

3.2 | siRNA-mediated depletion of EREG and PD98059 treatment blocks the ERK1/2 signaling pathway in AMI rats

Reverse transcription-quantitative PCR (RT-qPCR) and western blot were used to observe the changes of EREG expression and the ratio of ERK1 to ERK2 as well as its phosphorylation in ischemic myocardium of rats in each group (Figure 2a–c). There was no significant difference in the ratio of ERK1 to ERK2 among each group. The PD98059, EREG-siRNA, model, NC, and PD98059+EREG-siRNA groups displayed significantly higher mRNA and protein expression of EREG and the extent of ERK1/2 phosphorylation versus the normal group ($p < 0.05$). Meanwhile, in comparison with the model and NC groups, the extent of ERK1/2 phosphorylation in the PD98059, EREG-siRNA, and PD98059+EREG-siRNA groups was significantly decreased ($p < 0.05$), and the EREG-siRNA group and the PD98059+EREG-siRNA group exhibited decreased mRNA and protein expression of EREG ($p < 0.05$). No remarkable difference was observed in the protein expression of EREG among the model, NC, and PD98059 groups. However, the extent of ERK1 and ERK2 phosphorylation in the PD98059+EREG-siRNA group was significantly downregulated in relative to the PD98059 group ($p < 0.05$), suggesting EREG silencing results in the inhibition of the ERK1/2 signaling pathway.

3.3 | siRNA-mediated depletion of EREG and PD98059 treatment impairs cardiac function in AMI rats

Echocardiography was used to determine and assess the rat morphological indexes (LVEDD, LVESD) and systolic function indicators (LVEF, LVFS), the results of which demonstrated that compared with the normal group, the PD98059, EREG-siRNA, model, and NC groups had elevated LVEDD and LVESD, with reductions in LVEF and LVFS (all $p < 0.05$). In addition, compared with the model and NC groups, the PD98059, EREG-siRNA, and PD98059+EREG-siRNA groups exhibited enhanced LVEDD and LVESD, as well as significantly reduced LVEF and LVFS (all $p < 0.05$). Moreover, compared with the PD98059 and EREG-siRNA groups, the PD98059+EREG-siRNA group demonstrated elevated LVEDD and LVESD and reduced LVEF and LVFS (all $p < 0.05$) (Table 2). Thus, aforementioned results indicated that cardiac function in rats with AMI is worsened after the depression of EREG and inhibition of the ERK1/2 signaling pathway.

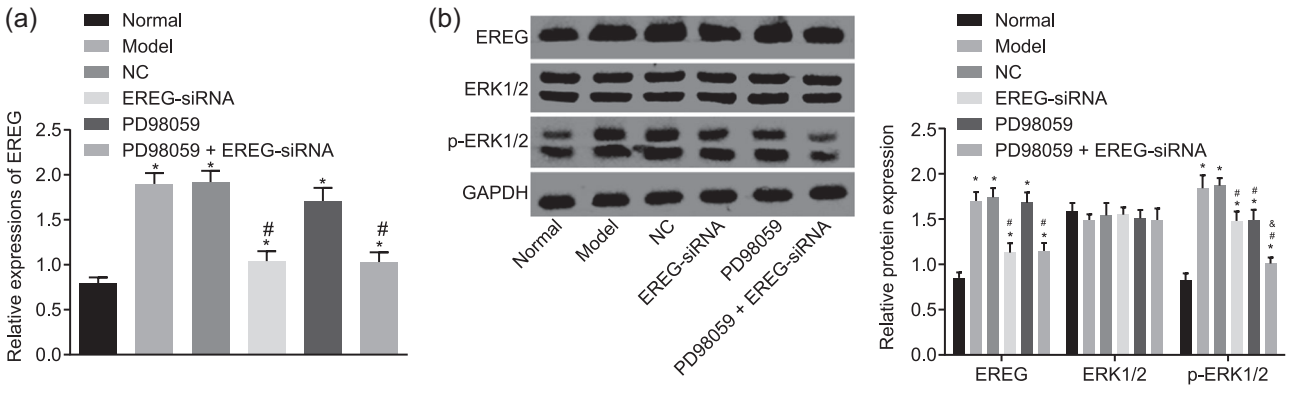

FIGURE 2 siRNA-mediated depletion of EREG and PD98059 treatment impedes the ERK1/2 signaling pathway in AMI rats. (a) The mRNA expression of EREG in response to the treatment of EREG-siRNA and/or PD98059 measured by RT-qPCR. (b) The protein expression of EREG, the ratio of ERK1 to ERK2, and its phosphorylation assessed by western blot analysis. (c) Quantification result from (b). $^{*}p < 0.05$ versus the normal group; $^{\#}p < 0.05$ versus the model group and the NC group; $^{\&}p < 0.05$ versus the PD98059 and EREG-siRNA groups. Measurement data were expressed as mean ± standard deviation, comparisons of which among multiple groups were assessed by one-way analysis of variance. $n = 10$. AMI: acute myocardial infarction; EREG: epiregulin; ERK1: extracellular-regulated protein kinases 1/2; GAPDH: glyceraldehyde-3-phosphate dehydrogenase; mRNA: messenger RNA; NC: negative control; RT-qPCR: reverse transcription-quantitative polymerase chain reaction; siRNA: small interfering RNA

3.4 | siRNA-mediated depletion of EREG and PD98059 treatment leads to myocardial injuries in AMI rats

Morphological characteristics of rats with AMI were analyzed using hematoxylin and eosin staining. In the normal group, the tissues displayed an even coloration of cardiac muscle fibers, with clear cell boundaries, well-aligned arrangement, distinct bands, normal myocardial cell form, no rupture of the myofilaments, uniform cell gaps, and without gathered and hyperplastic fibroblasts among muscle fibers. Whereas tissues in the model group and NC group exhibited a great loss of myocardial cells, with the viable cardiomyocytes disorganized with broken fibers, fibrous tissue hyperplasia as well as an enlarged necrotic region. In addition, the myocardial structure in the necrotic margin was observed to be damaged with a notable degree of inflammatory cell infiltration. Simultaneously, the PD98059 and EREG-siRNA groups were observed to have an enlarged area of myocardial necrosis, obviously broken fibers, a greater degree of inflammatory cell infiltration in contrast to the model group, and disordered myocardial arrangement at the edge of MI. Whereas the PD98059+EREG-siRNA group exhibited large areas of myocardial necrosis, severe fibrosis, increased inflammatory cell infiltration, MI edge disorder, and hypertrophy (Figure 3). Taken together, the aforementioned results demonstrated that the area of myocardial necrosis, fibrosis, and inflammatory cell infiltration are aggravated by depression of EREG and inhibition of the ERK1/2 signaling pathway.

3.5 | siRNA-mediated depletion of EREG and PD98059 treatment results in LV systolic and diastolic dysfunctions in AMI rats

Hemodynamic parameters (LVSP, LVEDP, LV+dp/dtmax, and LV−dp/dtmax) were determined, with the results indicating that compared with the normal group, the remaining groups exhibited decreased LVSP, LV+dp/dtmax, and LV−dp/dtmax and elevated LVEDP (all $p < 0.05$), suggesting damaged LV systolic function after AMI. In addition, compared with the model and NC groups, the PD98059, EREG-siRNA, and PD98059+EREG-siRNA groups exhibited significantly diminished LVSP, LV+dp/dtmax, and LV−dp/dtmax (all $p < 0.05$), which demonstrated intensified damage to LV systolic function, accompanied by significantly increased LVEDP ($p < 0.05$), suggesting damaged diastolic function among the rats. At the same time, compared with the PD98059 and EREG-siRNA groups, the PD98059+EREG-siRNA group presented with significantly downregulated LVSP, LV+dp/dtmax, and LV−dp/dtmax (all $p < 0.05$) as well as remarkably upregulated LVEDP (all $p < 0.05$), which demonstrated the aggravated MI-injured diastolic function. LVSP, LVEDP, LV+dp/dtmax, and LV−dp/dtmax data are depicted in Table 3. Therefore, LV systolic and diastolic function of rats with AMI was observed to be damaged by depression of EREG and inactivation of the ERK1/2 signaling pathway.

3.6 | siRNA-mediated depletion of EREG and PD98059 treatment inhibits angiogenesis in AMI rats

Numerous reports have identified CD31-positive expression as a marker of mature blood vessels (Luttun et al., 2002, Tateishi-Yuyama et al., 2002), and α-SAM-positive expression has been shown to be an indicator of angiogenesis. We subsequently determined the expression of CD31 and α-SMA in the tissues of rats by immunofluorescence. The results revealed that the green area represented positive staining of CD31 and the red area represented positive staining of α-SMA. Positive staining of both factors was represented by yellow. In addition, no newly formed vessels were detected, with the majority of vessels observed to be mature vessels with large lumen in the normal group. In the model group and the NC group, a large number of new vessels in clusters were observed, which were labeled with $CD31^+$ and $\alpha\text{-SMA}^+$, indicating that the new vessels covered by vascular endothelial cells were mature vessels. A few newly formed vessels were observed in the PD98059 group and the EREG-siRNA group. In the PD98059+EREG-siRNA group, a small number of new vessels were formed, and the lumen was covered with endothelial cells, which were immature vessels (Figure 4a). At the same time, CD31-positive microvessel density (MVD), α-SMA-positive MVD as

TABLE 2 Echocardiographic assessment of cardiac function

Group	LVEDD (mm)	LVESD (mm)	LVEF (%)	LVFS (%)
Normal	6.24 ± 0.41	3.05 ± 0.36	67.32 ± 6.78	52.77 ± 2.95
Model	8.96 ± 0.83*	6.56 ± 0.44*	28.61 ± 2.39*	21.09 ± 3.79*
NC	8.83 ± 0.37*	6.32 ± 0.58*	28.28 ± 4.01*	21.66 ± 3.82*
EREG-siRNA	10.13 ± 0.65*,#	7.48 ± 0.35*,#	17.73 ± 2.14*,#	14.43 ± 2.27*,#
PD98059	10.26 ± 0.71*,#	7.40 ± 0.48*,#	17.47 ± 1.59*,#	14.88 ± 2.98*,#
PD98059+EREG-siRNA	11.27 ± 0.35*,#,&	8.40 ± 0.39*,#,&	10.48 ± 0.49*, #, &	9.27 ± 3.02*,#,&

Note. Measurement data were expressed as mean ± standard deviation, and comparisons of which among multiple groups were assessed by one-way analysis of variance. EREG: epiregulin; LEVF: left ventricular ejection fraction; LVEDd: left ventricular end-diastolic diameter; LVESd: left ventricular end-systolic diameter; LVFS: left ventricular fractional shortening; NC: negative control; siRNA: small interfering RNA.

*$p < 0.05$ versus the normal group.

#$p < 0.05$ versus the model group and the NC group.

&$p < 0.05$ versus the PD98059 group and EREG-siRNA group.

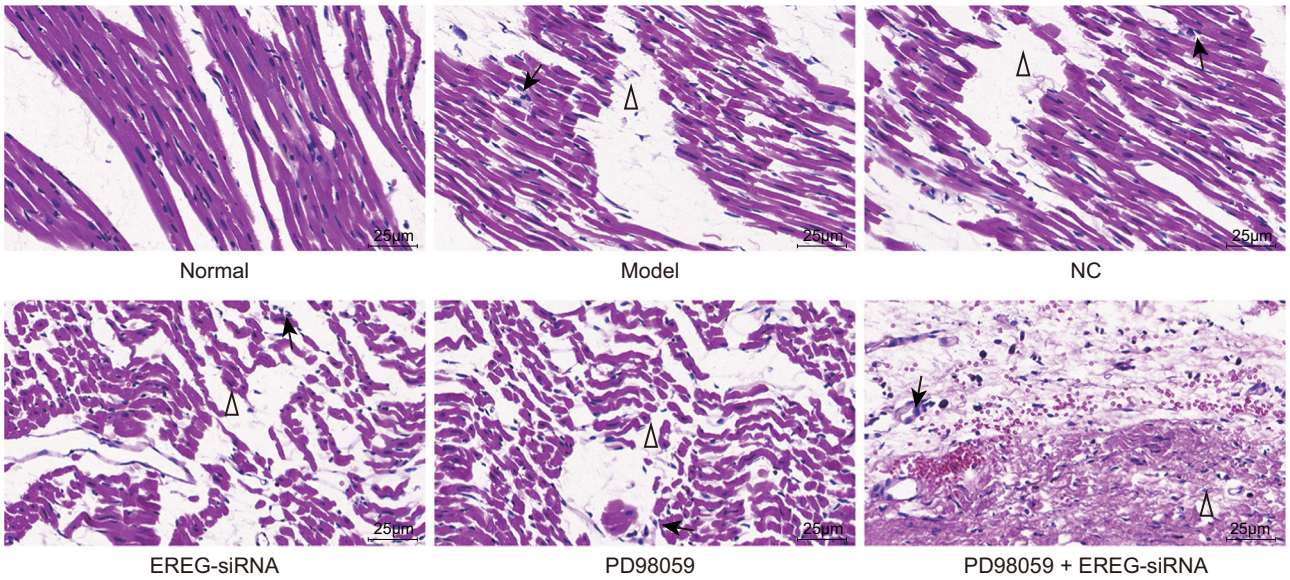

FIGURE 3 siRNA-mediated depletion of EREG and PD98059 treatment contributes to myocardial injuries and left ventricular remodeling in AMI rats (×200). The arrow indicates inflammatory cell infiltration, and the triangle indicates the area of myocardial necrosis. AMI: acute myocardial infarction; EREG: epiregulin; NC: negative control; siRNA: small interfering RNA [Color figure can be viewed at wileyonlinelibrary.com]

well as vascular maturity index (VMI; Figure 4b,c) were identified. In comparison with the normal group, the other groups all displayed enhanced MVD and VMI (all $p < 0.05$). Compared with the model and NC groups, the PD98059 and EREG-siRNA groups displayed a diminished MVD and VMI (all $p < 0.05$). The MVD and VMI in the PD98059+EREG-siRNA group were the lowest ($p < 0.05$), which was consistent with the immunofluorescence results. Hence, the silencing of EREG gene suppresses angiogenesis in rats with AMI.

3.7 | siRNA-mediated depletion of EREG and PD98059 treatment enlarges infarct size in AMI rats

The MI region was analyzed using the TTC assay, the results of which (Figure 5a,b) indicated that MI areas in the PD98059, EREG-siRNA, model, NC, and PD98059+EREG-siRNA groups were larger than that in the normal group (all $p < 0.05$). In addition, when compared with the model and NC groups, the PD98059, EREG-siRNA, and PD98059+EREG-siRNA groups demonstrated a significantly enhanced MI area (all $p < 0.05$). At the same time, when compared with the PD98059 and EREG-siRNA groups, the PD98059+EREG-siRNA group exhibited elevated MI area (all $p < 0.05$). Therefore, on the basis of the results, MI area is enlarged through silencing of EREG and suppression of the ERK1/2 signaling pathway.

3.8 | siRNA-mediated depletion of EREG and PD98059 treatment promotes left ventricular cardiomyocyte loss

TUNEL staining (Figure 6) was used to determine myocardial cell apoptosis. The apoptotic cell was observed with tan-stained nuclei. TUNEL-positive cells were seldom observed in normal myocardial cells, which were presented with blue coloration because of

TABLE 3 Assessment of hemodynamic performance

Group	LVSP (mmHg)	LVEDP (mmHg)	LV + dp/dtmax (mmHg/s)	LV−dp/dtmax (mmHg/s)
Normal	153.56 ± 6.52	13.79 ± 1.97	6364.12 ± 65.32	5552.72 ± 43.65
Model	93.35 ± 7.31*	18.45 ± 1.18*	3767.36 ± 12.09*	3523.78 ± 41.56*
NC	89.12 ± 6.79*	18.82 ± 0.71*	3818.16 ± 25.06*	3418.92 ± 38.09*
EREG-siRNA	77.74 ± 5.93*,#	20.55 ± 0.15*,#	3157.21 ± 33.60*,#	2804.44 ± 15.19*,#
PD98059	76.69 ± 5.01*,#	20.63 ± 0.41*,#	3021.89 ± 23.12*,#	2802.78 ± 27.84*,#
PD98059+EREG-siRNA	53.32 ± 6.91*,#,&	25.65 ± 0.63*,#, &	2241.11 ± 35.57*,#,&	20662.45 ± 22.07*,#,&

Note. Measurement data were expressed as mean ± standard deviation, and comparisons of which among multiple groups were assessed by one-way analysis of variance. $n = 10$. LV+dp/dtmax: left ventricular maximum increase and decrease rate; LVEDP: left ventricular end-diastolic pressure; LVSP: left ventricular systolic pressure; NC: negative control.

*$p < 0.05$ versus the normal group.

#$p < 0.05$ versus the model group and the NC group.

&$p < 0.05$ versus the PD98059 group and EREG-siRNA group.

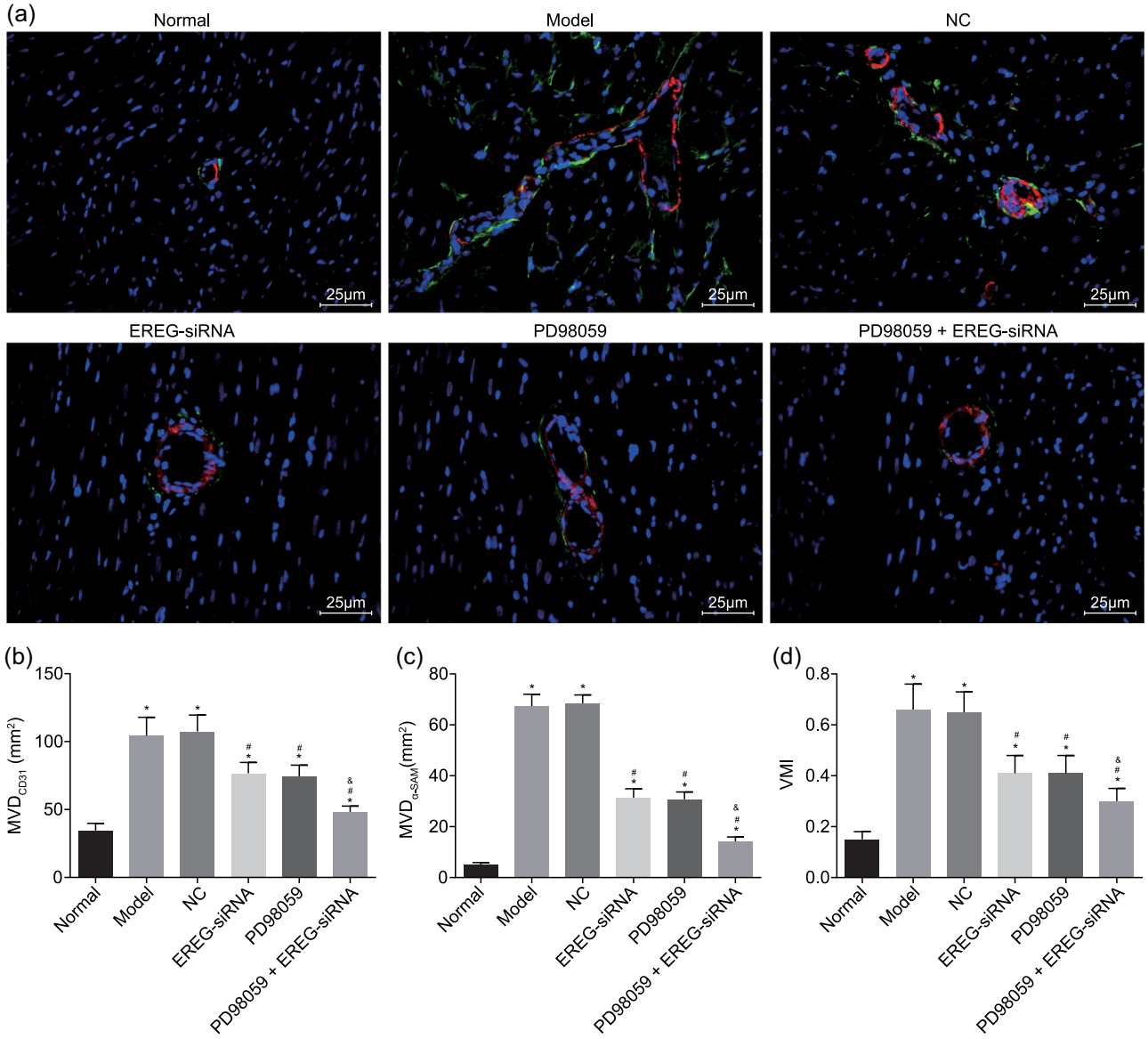

FIGURE 4 siRNA-mediated depletion of EREG and PD98059 treatment represses angiogenesis in AMI rats. (a) Immunofluorescence staining of CD31 and α-SAM (×400); (b) MVD_{CD31} in response to the treatment of EREG-siRNA and/or PD98059; (c) $MVD_{α-SAM}$ in response to the treatment of EREG-siRNA and/or PD98059; (d) VMI ($MVD_{α-SAM}/MVD_{CD31}$) in response to the treatment of EREG-siRNA and/or PD98059; $^*p < 0.05$ versus the normal group; $^\#p < 0.05$ versus the model group and the NC group; $^\&p < 0.05$ versus the PD98059 group and EREG-siRNA group. Measurement data were expressed as mean ± standard deviation, comparisons of which among multiple groups were assessed by one-way analysis of variance. $n = 10$. AMI: acute myocardial infarction; EREG: epiregulin; ERK1: extracellular-regulated protein kinases 1/2; MVD: microvessel density; MVD_{CD31}: CD31-positive MVD; $MVD_{α-SAM}$: α-SMA-positive MVD; NC: negative control; siRNA: small interfering RNA; VMI: vascular maturity index; α-SMA: α-smooth muscle actin [Color figure can be viewed at wileyonlinelibrary.com]

hematoxylin staining, in addition to relatively larger nucleus and the same morphological size. Compared with the normal group, the PD98059, EREG-siRNA, model, NC, and PD98059+EREG-siRNA groups displayed significantly elevated apoptotic cells (all $p < 0.05$). In comparison with the model and NC groups, the PD98059+EREG-siRNA, PD98059, and EREG-siRNA groups exhibited increased apoptotic cells ($p < 0.05$). In addition, compared with the PD98059 group and the EREG-siRNA group, the PD98059+EREG-siRNA group showed obviously increased apoptotic cells ($p < 0.05$). Thus, we could conclude that cell apoptosis was promoted by the downregulation of EREG and inhibition of the ERK1/2 signaling pathway.

3.9 | siRNA-mediated depletion of EREG and PD98059 treatment reduces expression of factors related to angiogenic capacity

The mRNA and protein expression of VEGF, bFGF, and IGF-I was analyzed using RT-qPCR and western blot analysis (Figure 7). Versus the normal group, the expression of VEGF, bFGF, and IGF-I was

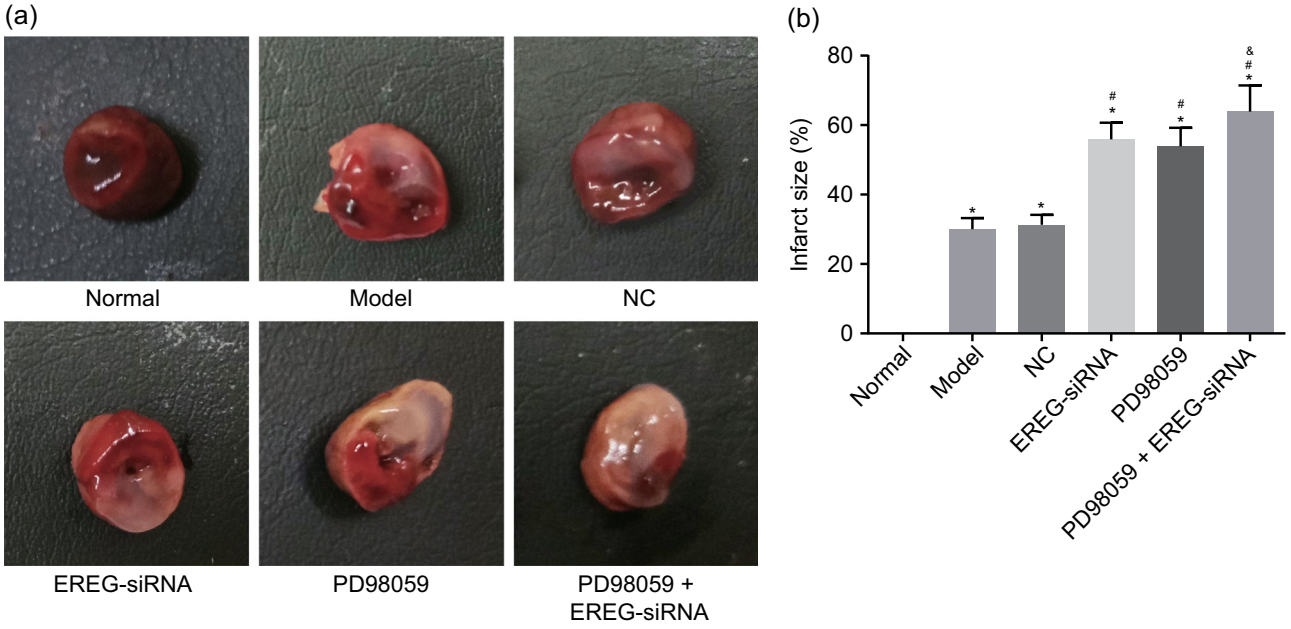

FIGURE 5 siRNA-mediated depletion of EREG and PD98059 treatment enlarges infarct size in AMI rats. (a) TTC staining showing MI area of rats after EREG silencing and/or inhibition of the ERK1/2 signaling pathway (×400); (b) quantification results from (a); $^{*}p < 0.05$ versus the normal group; $^{\#}p < 0.05$ versus the model group and the NC group; $^{\&}p < 0.05$ versus the PD98059 group and EREG-siRNA group. Measurement data were expressed as mean ± standard deviation, comparisons of which among multiple groups were assessed by one-way analysis of variance. $n = 10$. AMI: acute myocardial infarction; EREG: epiregulin; ERK1: extracellular-regulated protein kinases 1/2; MI: myocardial infarction; NC: negative control; siRNA: small interfering RNA; TCC: 2,3,5-triphenyl-2H-tetrazolium chloride [Color figure can be viewed at wileyonlinelibrary.com]

elevated in the EREG-siRNA model, NC, and PD98059+EREG-siRNA groups (all $p < 0.05$). In addition, in comparison with the model and NC groups, the PD98059, EREG-siRNA, and PD98059+EREG-siRNA groups displayed diminished expression of VEGF, bFGF, and IGF-I (all $p < 0.05$). Simultaneously, the expression of VEGF, bFGF, and IGF-I exhibited a significant decline in the PD98059+EREG-siRNA group when compared with the PD98059 and EREG-siRNA groups (all $p < 0.05$). The results suggested that the expression of VEGF, bFGF, and IGF-I was downregulated when EREG was silenced and the ERK1/2 signaling pathway was blocked.

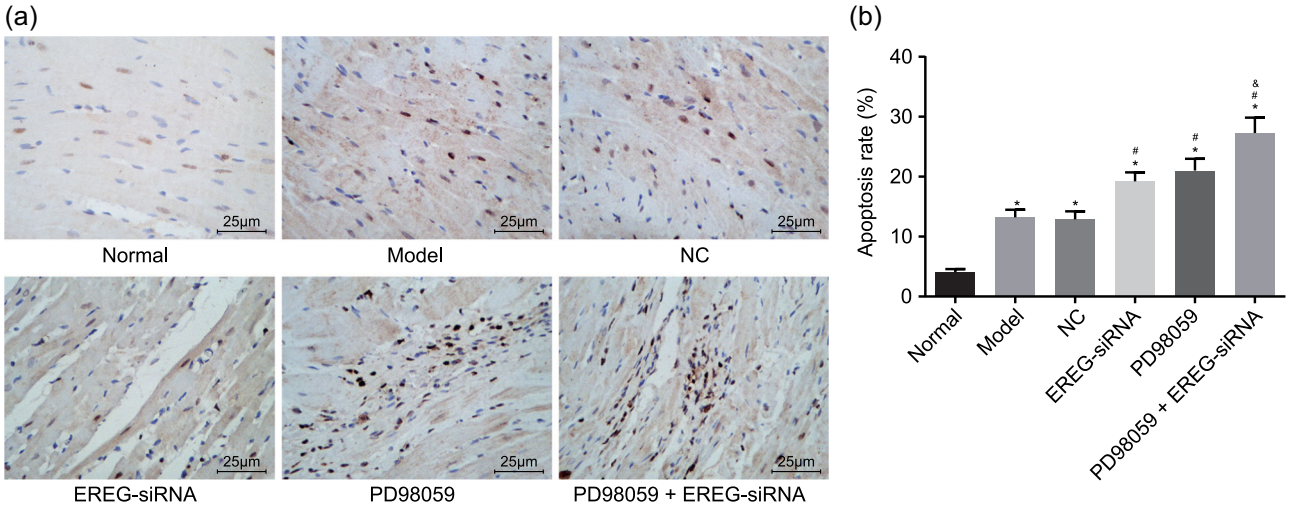

FIGURE 6 siRNA-mediated depletion of EREG and PD98059 treatment enhances left ventricular cardiomyocyte apoptosis. (a) TUNEL staining demonstrating the myocardial cell apoptosis in rats after EREG silencing and/or inhibition of the ERK1/2 signaling pathway; (b) myocardial cell apoptosis rate in rats after EREG silencing and/or inhibition of the ERK1/2 signaling pathway; $^{*}p < 0.05$ versus the normal group; $^{\#}p < 0.05$ versus the model group and the NC group; $^{\&}p < 0.05$ versus the PD98059 group and EREG-siRNA group. Measurement data were expressed as mean ± standard deviation, comparisons of which among multiple groups were assessed by one-way analysis of variance. $n = 10$. EREG: epiregulin; ERK1: extracellular-regulated protein kinases 1/2; NC: negative control; siRNA: small interfering RNA; TUNEL: TdT-mediated dUTP-biotin nick-end labeling [Color figure can be viewed at wileyonlinelibrary.com]

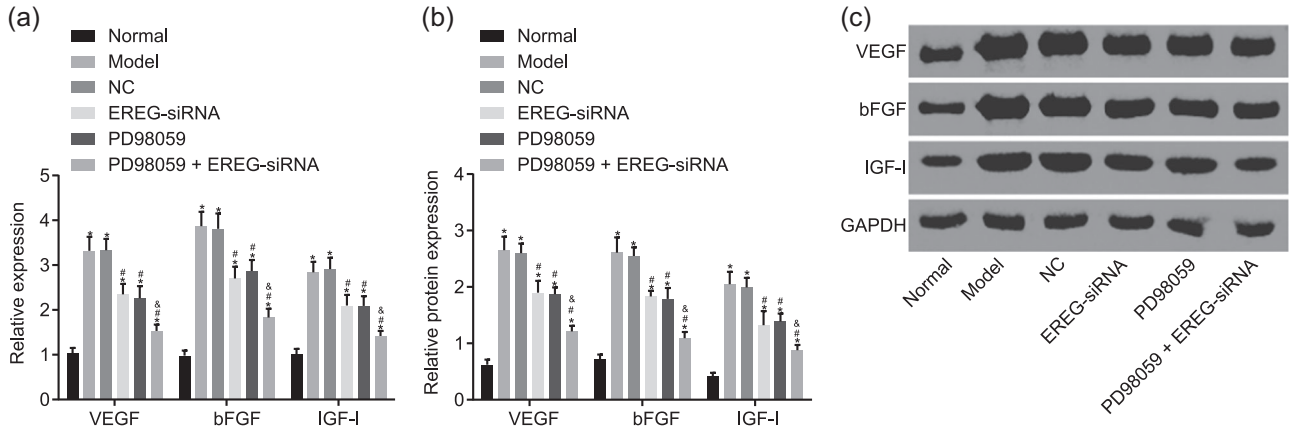

FIGURE 7 siRNA-mediated depletion of EREG and PD98059 lowers pertinent factors in relation to angiogenic capacity. (a) The mRNA expression of VEGF, bFGF, and IGF-I measured by RT-qPCR after EREG silencing and/or inhibition of ERK1/2 signaling pathway. (b) The protein expression of VEGF, bFGF, and IGF-I evaluated by western blot analysis after EREG silencing and/or inhibition of ERK1/2 signaling pathway. (c) Gray value of VEGF, bFGF, and IGF-I protein bands after EREG silencing and/or inhibition of ERK1/2 signaling pathway. $^{*}p < 0.05$ versus the normal group; $^{\#}p < 0.05$ versus the model group and the NC group; $^{\&}p < 0.05$ versus the PD98059 group and EREG-siRNA group. Measurement data were expressed as mean ± standard deviation, comparisons of which among multiple groups were assessed by one-way analysis of variance. $n = 10$. bFGF: basic fibroblast growth factor; EREG: epiregulin; ERK1/2: extracellular-regulated protein kinases 1/2; IGF-I: insulin-like growth factor I; NC: negative control; RT-qPCR: reverse transcription-quantitative polymerase chain reaction; siRNA: small interfering RNA; VEGF: vascular endothelial growth factor

4 | DISCUSSION

AMI represents one of the most devastating cardiovascular diseases and continues to cause high morbidity and mortality worldwide, partly due to its elevated arrhythmogenicity (S. Liu et al., 2016; X. Liu et al., 2016). According to an estimate by the World Bank, the annual number of patients suffering from AMI in China will reach approximately 23 million by the year 2030 (Zhang et al., 2015). A recent study highlighted the crucial role played by EREG in mediating liver regeneration along with the mitogenic activity of vasoactive antagonists in smooth muscle cells involved in the process of reproduction, with highly localized expression in the macrophages, uterus of early pregnancy, ovary, and placenta (D. Lee et al., 2004). In an attempt to investigate the potential role of EREG and its involvement in rat models of AMI, angiogenesis and ventricular remodeling were evaluated after siRNA-mediated EREG silencing. Collectively, the findings of the current study revealed that EREG was highly expressed in rats with AMI, and silencing of which restrained angiogenesis and augmented ventricular remodeling in rats with AMI via inhibiting activation of the ERK1/2 signaling pathway.

Initially, high levels of EREG were detected in rats with AMI. A recent study implicated high expression of EREG in a variety of human cancers, including pancreatic cancer, colon cancer, breast cancer, bladder cancer, and non-small-cell lung cancer (Sunaga et al., 2013). Moreover, the elevated tumor gene expression of EREG and AREG, encoding the ligands to EGFR, such as EREG and AREG, has been linked with a good efficacy of anti-EGFR treatment in metastatic colorectal cancer (M.S. Lee et al., 2016). Furthermore, a previous report demonstrated that EREG acts as an inducer of ErbB-dependent signaling networks in tumor, binding to ErbB1 which ultimately contributes to higher mitogenic potential (Auf et al., 2013). In addition, upregulated EREG in esophageal cancer cells has been reported to contribute to reduced survival times in vivo and promote lung metastasis (Sun et al., 2016). In the current study, we investigated the expression of EREG with siRNA, which demonstrated involvement in various cellular biological processes as well as cardiac function and angiogenesis.

Evidence was subsequently obtained suggesting that silencing of the EREG gene restrained the activation of the ERK1/2 signaling pathway, contributing to enhancements in myocardial necrosis, fibrosis, and inflammatory cell infiltration, all of which elevated myocardial cell apoptosis in AMI rats. Treating salivary adenoid cystic carcinoma cells with recombinant human EREG (rhEREG) in a previous study resulted in an induced extent of EGFR and ERK phosphorylation in a time- and dose-dependent manner (S. Liu et al., 2016; X. Liu et al., 2016). A previous study identified similar observations whereby EREG was found to promote the differentiation of dental pulp mesenchymal stem cells by activating the MEK/ERK and JNK signaling pathways (Cao et al., 2013), suggesting the ability of EREG to influence the expression of ERK. Interestingly, another study revealed that the development of cardiac remodeling could be attenuated through the inhibition of the MEK–ERK1/2 signaling pathway.

Most important, the findings of the current study revealed that silencing of the EREG gene silencing impeded angiogenesis and promoted ventricular remodeling of rats with AMI, as attributed from a decreased number of new blood vessels as well as a decreased left ventricular systolic and diastolic function. Angiogenesis is a complex process involved in reproduction, development, and wound healing, which can be modulated by various angiogenic activators and inhibitors (Park et al., 2005). Low-power laser-irradiation-induced

VEGF production was inhibited by suppressing the activity of ERK, illustrating the expression of VEGF was modulated by the ERK signaling pathway, which may be closely related to the cell proliferation and angiogenesis (Feng, Zhang, & Xing, 2012). When ERK responds to certain signals, such as focal adhesion kinase (J. Lee, Borboa, Chun, Baird, & Eliceiri, 2010), the activation of the ERK signaling pathway promotes cell proliferation or survival; if the cell continues to proliferate and does not migrate, the vascular structure of endothelial cells accumulates and forms the capsule cavity. Ventricular remodeling refers to a process after MI, with an elevated risk of heart failure, where the heart experiences progressive LV diastolic and systolic dysfunction (Gao et al., 2013). EREG has been reported to have a positive impact on wound healing, oocyte maturation, inflammation, and tissue repair through stimulating cell proliferation together with regulating angiogenesis and vascular remodeling (Riese & Cullum, 2014).

In conclusion, the present study suggests that silencing of the EREG contributes to enhanced myocardial cell apoptosis, repressed angiogenesis, and increased ventricular remodeling in rats with AMI through the suppression of the ERK1/2 signaling pathway (Figure S1). Importantly, our study revealed that EREG is silenced by siRNA and thus inhibiting the activation of the ERK1/2 signaling pathway. We observed that in response to ERK1/2 signaling pathway repression, angiogenesis was restrained in rats with AMI, as reflected by decreased MVD and VMI, as well as downregulated expression of bFGF, IGF-I, and VEGF. Meanwhile, EREG gene silencing induced ventricular remodeling with the presence of constrained LV systolic and diastolic function by suppressing the ERK1/2 signaling pathway. These findings may provide a fresh perspective for future AMI treatments that may improve the life quality of patients suffering from AMI. However, the current study primarily focused on the role of EREG in the angiogenesis and left vascular remodeling, the potential mechanism underlying the release of inflammatory cytokines remains to be explored in future investigations.

ACKNOWLEDGMENTS

We would like to thank our researchers for their hard work and reviewers for their valuable advice.

CONFLICT OF INTERESTS

The authors declare that they have no conflict of interests.

AUTHOR CONTRIBUTIONS

Y. C. and H.-L. W. designed the study. K.-L. X. and K. W. collated the data, designed and developed the database, carried out data analyses, and produced the initial draft of the manuscript. Y. C., K.-L. X., H.-L. W., and K. W. contributed to drafting and polishing the manuscript. All authors have read and approved the final submitted manuscript.

ORCID

Kai Wu http://orcid.org/0000-0003-4835-8741

REFERENCES

Auf, G., Jabouille, A., Delugin, M., Guérit, S., Pineau, R., North, S., … Moenner, M. (2013). High epiregulin expression in human U87 glioma cells relies on IRE1alpha and promotes autocrine growth through EGF receptor. *BMC Cancer*, *13*, 597.

Cao, Y., Xia, D. S., Qi, S. R., Du, J., Ma, P., Wang, S. L., & Fan, Z. P. (2013). Epiregulin can promote proliferation of stem cells from the dental apical papilla via MEK/Erk and JNK signalling pathways. *Cell Proliferation*, *46*(4), 447–456.

Du, C. Q., Yang, L., Han, J., Yang, J., Yao, X. Y., Hu, X. S., & Hu, S. J. (2012). The elevated serum S100A8/A9 during acute myocardial infarction is not of cardiac myocyte origin. *Inflammation*, *35*(3), 787–796.

Fang, L., Cheng, J. C., Chang, H. M., Sun, Y. P., & Leung, P. C. (2013). EGF-like growth factors induce COX-2-derived PGE2 production through ERK1/2 in human granulosa cells. *The Journal of Clinical Endocrinology and Metabolism*, *98*(12), 4932–4941.

Feng, J., Zhang, Y., & Xing, D. (2012). Low-power laser irradiation (LPLI) promotes VEGF expression and vascular endothelial cell proliferation through the activation of ERK/Sp1 pathway. *Cellular Signalling*, *24*(6), 1116–1125.

Gao, Y., Li, T., Wu, C., Bittle, G. J., Chen, S., Wu, Z. J., & Griffith, B. P. (2013). Pim-1 mediated signaling during the process of cardiac remodeling following myocardial infarction in ovine hearts. *Journal of Molecular and Cellular Cardiology*, *63*, 89–97.

Jia, K., Shi, P., Han, X., Chen, T., Tang, H., & Wang, J. (2016). Diagnostic value of miR-30d-5p and miR-125b-5p in acute myocardial infarction. *Molecular Medicine Reports*, *14*(1), 184–194.

Kohsaka, S., Hinohara, K., Wang, L., Nishimura, T., Urushido, M., Yachi, K., … Tanaka, S. (2014). Epiregulin enhances tumorigenicity by activating the ERK/MAPK pathway in glioblastoma. *Neuro-Oncology*, *16*(7), 960–970.

Lake, D., Correa, S. A., & Muller, J. (2016). Negative feedback regulation of the ERK1/2 MAPK pathway. *Cellular and Molecular Life Sciences*, *73*(23), 4397–4413.

Lee, D., Pearsall, R. S., Das, S., Dey, S. K., Godfrey, V. L., & Threadgill, D. W. (2004). Epiregulin is not essential for development of intestinal tumors but is required for protection from intestinal damage. *Molecular and Cellular Biology*, *24*(20), 8907–8916.

Lee, J., Borboa, A. K., Chun, H. B., Baird, A., & Eliceiri, B. P. (2010). Conditional deletion of the focal adhesion kinase FAK alters remodeling of the blood-brain barrier in glioma. *Cancer Research*, *70*(24), 10131–10140.

Lee, M. S., McGuffey, E. J., Morris, J. S., Manyam, G., Baladandayuthapani, V., Wei, W., … Kopetz, S. (2016). Association of CpG island methylator phenotype and EREG/AREG methylation and expression in colorectal cancer. *British Journal of Cancer*, *114*(12), 1352–1361.

Liu, S., Ye, D., Xu, D., Liao, Y., Zhang, L., Liu, L., … Zhang, Z. (2016). Autocrine epiregulin activates EGFR pathway for lung metastasis via EMT in salivary adenoid cystic carcinoma. *Oncotarget*, *7*(18), 25251–25263.

Liu, X., Zhang, Y., Du, W., Liang, H., He, H., Zhang, L., … Shan, H. (2016). MiR-223-3p as a novel microRNA regulator of expression of voltage-gated K+ channel Kv4.2 in acute myocardial infarction. *Cellular Physiology and Biochemistry*, *39*(1), 102–114.

Luttun, A., Tjwa, M., Moons, L., Wu, Y., Angelillo-Scherrer, A., Liao, F., … Carmeliet, P. (2002). Revascularization of ischemic tissues by PlGF treatment, and inhibition of tumor angiogenesis, arthritis and atherosclerosis by anti-Flt1. *Nature Medicine*, *8*(8), 831–840.

Machulsky, N. F., Barchuk, M., Gagliardi, J., Gonzalez, D., Lombardo, M., Escudero, A. G., … Berg, G. (2017). Vitamin D is related to markers of vulnerable plaque in acute myocardial infarction. *Current Vascular Pharmacology*, 355–360.

Martin, L. J., Smith, S. B., Khoutorsky, A., Magnussen, C. A., Samoshkin, A., Sorge, R. E., … Diatchenko, L. (2017). Epiregulin and EGFR interactions are involved in pain processing. *The Journal of Clinical Investigation*, *127*(9), 3353–3366.

Mikhail, C., Vaucher, A., Jimenez, S., & Tafti, M. (2017). ERK signaling pathway regulates sleep duration through activity-induced gene expression during wakefulness. *Science Signaling*, *10*, 463.

Neri, M., Riezzo, I., Pascale, N., Pomara, C., & Turillazzi, E. (2017). Ischemia/reperfusion injury following acute myocardial infarction: A critical issue for clinicians and forensic pathologists. *Mediators of Inflammation*, *2017*, 7018393.

Oyama, J., Blais, C., Jr., Liu, X., Pu, M., Kobzik, L., Kelly, R. A., & Bourcier, T. (2004). Reduced myocardial ischemia-reperfusion injury in toll-like receptor 4-deficient mice. *Circulation*, *109*(6), 784–789.

Park, J. E., Lee, D. H., Lee, J. A., Park, S. G., Kim, N. S., Park, B. C., & Cho, S. (2005). Annexin A3 is a potential angiogenic mediator. *Biochemical and Biophysical Research Communications*, *337*(4), 1283–1287.

Riese, D. J., 2nd, & Cullum, R. L. (2014). Epiregulin: Roles in normal physiology and cancer. *Seminars in Cell & Developmental Biology*, *28*, 49–56.

Seropian, I. M., Toldo, S., Van Tassell, B. W., & Abbate, A. (2014). Anti-inflammatory strategies for ventricular remodeling following ST-segment elevation acute myocardial infarction. *Journal of the American College of Cardiology*, *63*(16), 1593–1603.

Shannon, P., Markiel, A., Ozier, O., Baliga, N. S., Wang, J. T., Ramage, D., … Ideker, T. (2003). Cytoscape: A software environment for integrated models of biomolecular interaction networks. *Genome Research*, *13*(11), 2498–2504.

Sivaraman, S. K., Zachariah, G., & Annamala, P. (2014). Effect of smoking on metalloproteinases (MMPs) activity in patients with acute myocardial infarction (AMI). *Journal of Clinical and Diagnostic Research*, *8*(2), 27–30.

Smyth, G. K. (2004). Linear models and empirical Bayes methods for assessing differential expression in microarray experiments. *Statistical Applications in Genetics and Molecular Biology*, *3*, 1–25.

Sun, L., Pan, J., Yu, L., Liu, H., Shu, X., Sun, L., … Ran, Y. (2016). Tumor endothelial cells promote metastasis and cancer stem cell-like phenotype through elevated epiregulin in esophageal cancer. *American Journal of Cancer Research*, *6*(10), 2277–2288.

Sunaga, N., Kaira, K., Imai, H., Shimizu, K., Nakano, T., Shames, D. S., … Mori, M. (2013). Oncogenic KRAS-induced epiregulin overexpression contributes to aggressive phenotype and is a promising therapeutic target in non-small-cell lung cancer. *Oncogene*, *32*(34), 4034–4042.

Tateishi-Yuyama, E., Matsubara, H., Murohara, T., Ikeda, U., Shintani, S., Masaki, H., … Therapeutic Angiogenesis using Cell Transplantation Study Investigators. (2002). Therapeutic angiogenesis for patients with limb ischaemia by autologous transplantation of bone-marrow cells: A pilot study and a randomised controlled trial. *Lancet*, *360*(9331), 427–435.

Wang, J., Huang, W., Xu, R., Nie, Y., Cao, X., Meng, J., … Zheng, Z. (2012). MicroRNA-24 regulates cardiac fibrosis after myocardial infarction. *Journal of Cellular and Molecular Medicine*, *16*(9), 2150–2160.

Wei, P., Yang, X. J., Fu, Q., Han, B., Ling, L., Bai, J., … Jiang, C. Y. (2015). Intermedin attenuates myocardial infarction through activation of autophagy in a rat model of ischemic heart failure via both cAMP and MAPK/ERK1/2 pathways. *International Journal of Clinical and Experimental Pathology*, *8*(9), 9836–9844.

Yu, Y., Wei, S. G., Zhang, Z. H., Weiss, R. M., & Felder, R. B. (2016). ERK1/2 MAPK signaling in hypothalamic paraventricular nucleus contributes to sympathetic excitation in rats with heart failure after myocardial infarction. *American Journal of Physiology Heart and Circulatory Physiology*, *310*(6), H732–H739.

Yuan, C., Yu, G., Yang, T., Li, W., Ai, Q., & Deng, L. (2013). Enhanced therapeutic effects on acute myocardial infarction with multiple intravenous transplantation of human cord blood mononuclear cells. *International Journal of Cardiology*, *168*(3), 2767–2773.

Yun, J., Song, S. H., Park, J., Kim, H. P., Yoon, Y. K., Lee, K. H., … Kim, T. Y. (2012). Gene silencing of EREG mediated by DNA methylation and histone modification in human gastric cancers. *Laboratory Investigation*, *92*(7), 1033–1044.

Zhang, L., Desai, N. R., Li, J., Hu, S., Wang, Q., Li, X., … China PEACE Collaborative Group. (2015). National quality assessment of early clopidogrel therapy in Chinese patients with acute myocardial infarction (AMI) in 2006 and 2011: Insights from the China patient-centered evaluative assessment of cardiac events (PEACE)-retrospective AMI study. *Journal of the American Heart Association*, *4*(7), e001906.

Zouggari, Y., Ait-Oufella, H., Bonnin, P., Simon, T., Sage, A. P., Guerin, C., … Mallat, Z. (2013). B lymphocytes trigger monocyte mobilization and impair heart function after acute myocardial infarction. *Nature Medicine*, *19*(10), 1273–1280.

SUPPORTING INFORMATION

Additional supporting information may be found online in the Supporting Information section at the end of the article.

How to cite this article: Cai Y, Xie K-L, Wu H-L, Wu K. Functional suppression of Epiregulin impairs angiogenesis and aggravates left ventricular remodeling by disrupting the extracellular-signal-regulated kinase1/2 signaling pathway in rats after acute myocardial infarction. *J Cell Physiol*. 2019; 1–13. https://doi.org/10.1002/jcp.28503